Second harmonic generation in ridge Bragg reflection waveguides

Bhavin Bijlani,[a] Payam Abolghasem, and A. S. Helmy
Edward Rogers, Sr. Department of Electrical and Computer Engineering, University of Toronto, Toronto, Ontario M5S 3G4, Canada

(Received 10 January 2008; accepted 18 February 2008; published online 13 March 2008)

Monolithic AlGaAs ridge Bragg reflection waveguides are used to achieve exact phase matching in a second harmonic generation experiment for a pump at 1600 nm. Phase-matching bandwidth of 4.5 nm, with a peak internal conversion efficiency of 205 %/W cm^2, is obtained. This conversion efficiency is comparable to numbers reported for periodically poled lithium niobate. The phase-matching peak was found to redshift with sample temperature providing tunablity at a rate of 0.25 nm/ °C. Possible routes for enhancing the current efficiency levels are also discussed. © *2008 American Institute of Physics*. [DOI: 10.1063/1.2894516]

Interest in the nonlinear optical properties of compound semiconductor materials is garnered by the promise of low-power frequency conversion via their relatively large nonlinear coefficient. Also, mature microfabrication technologies may allow for fully integrated nonlinear conversion devices with self contained pump sources on chip. Unfortunately, utilizing the second-order optical nonlinearity is hindered by the lack of a natural phase-matching mechanism. Many techniques have been examined recently to artificially enable phase matching. These are often studied for second-harmonic generation (SHG) experiments due to the ease of the experimental setup involved. Some technologies such as modal phase matching[1] and form birefringence[2] exploit waveguide dispersion to achieve phase matching. Other technologies such as quasi-phase matching[3] use periodic modulation of the nonlinear coefficient in the propagation direction to compensate for the phase mismatch.

Recently, a technique has been devised to allow phase matching in semiconductors which is akin to modal phase matching.[4] This technique utilizes a structure that can support guided modes via both total internal reflection (TIR) and transverse Bragg reflection (TBR). The latter occurs by distributed reflection from mirrors above and below a core such that there is optical confinement within the core. By phase matching the fundamental modes of both types, TIR and TBR, efficient phase matching and hence frequency conversion can take place. The benefit of this method over others is its potential for providing low loss at both wavelengths of interest as well as being more amenable to monolithic integration. Recently, we have demonstrated phase-matched SHG in slab Bragg reflection waveguides with modest conversion efficiencies on the order of 0.1 %/W.[5] Here, we report the demonstration of SHG via ridge BRWs. A schematic of this type of waveguide is shown in Fig. 1 along with an intensity profile of both the fundamental TBR and TIR modes. The enhanced intensity within the ridge waveguide in comparison to modes in slab waveguides serves to substantially enhance the conversion efficiency. The ridge structure also influences other phase matching (PM) parameters such as the bandwidth, as will be discussed.

The wafer used was grown nominally undoped using metal-organic chemical vapor deposition on semi-insulating GaAs substrate. The upper and lower reflectors were grown with eight and ten periods, respectively. Each period consists of an $Al_{0.6}Ga_{0.4}As$ layer with a thickness of 278 nm of and an $Al_{0.2}Ga_{0.8}As$ layer with a thickness of 118 nm. The $Al_{0.4}Ga_{0.6}As$ core thickness is 328 nm. Sections of approximately 5×5 mm^2 were then patterned from the wafer and etched using a photoresist mask and a low-power BCl_3/Ar reactive ion etch process to a depth of ~4 μm just past the core layer as depicted in Fig. 1. The resulting ridges had widths of approximately ~3 μm. The sample was cleaved to a length of 2.12 mm.

Using an end-fire coupling setup, the samples were initially characterized for linear loss using a C-band tunable distributed feedback laser-diode source. The propagation loss at 1555 nm was measured to be 5.9 ± 0.2 cm^{-1} using the Fabry–Pérot method. This value is higher than our reported slab value and is likely due to the roughness from the deep etch.[5]

The SHG was characterized using a pulsed optical parametric oscillator source pumped by a mode-locked Ti:Sapphire, also with an end-fire coupling setup. The output pulses had a temporal full width at half maximum (FWHM) of 2 ps, a repetition frequency of 75.6 MHz and spectral FWHM of ~3–4 nm. The average output power was typically

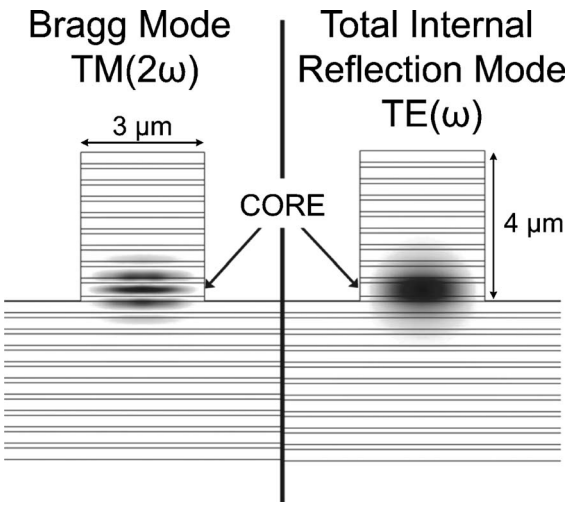

FIG. 1. Intensity maps of the modes used in this work. The dimensions of the fabricated structure are indicated.

[a]Electronic mail: b.bijlani@utoronto.ca.

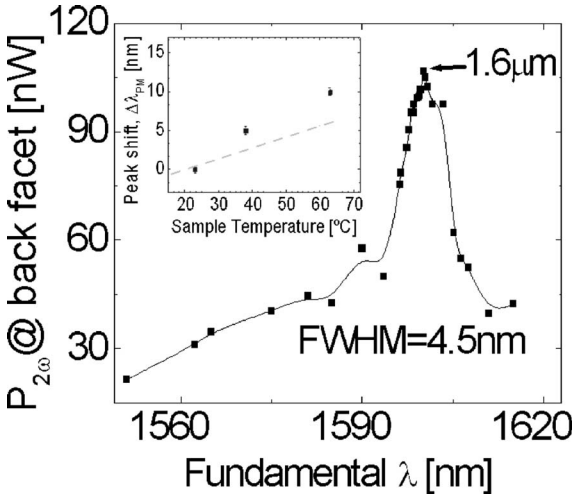

FIG. 2. Phase-matching tuning curve revealing a distinct peak at ~1600 nm with FWHM of 4.5 nm. The peak is modulated by FP fringes of the fundamental. The phase-matching peak is shown to redshift, by the value $\Delta\lambda_{PM}$, with increasing temperature at a rate of 0.25 nm/ °C (inset, black dots). The gray line (inset) is the theoretical simulation. Powers shown are inside the sample.

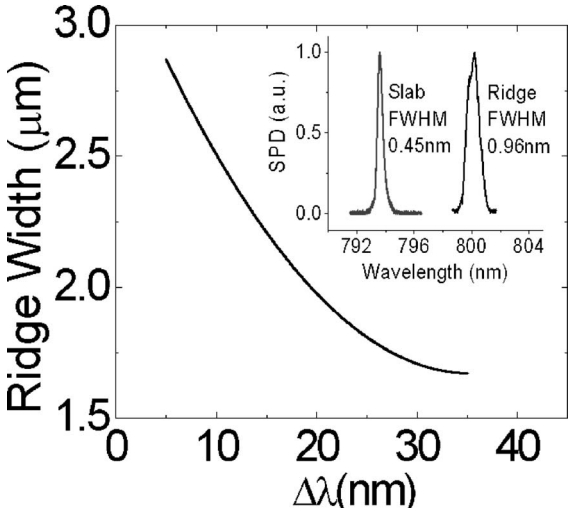

FIG. 3. Simulated ridge width *W vs* phase-matching wavelength shift from the case of the slab, Δλ. For a waveguide width $W=3$ μm, fabrication-induced variation in the mask width can account for spectral broadening. Inset: comparison second-harmonic spectra at phase-matching for the slab (left) and ridge (right) cases.

200 mW. The sample was mounted on a temperature controlled stage.

Prior to conducting the SHG experiments, confirmation of the significant contribution of two-photon absorption was observed at high intensities (average input powers above 25 mW at the facet). Using low input fundamental power (21 mW at the facet) where this absorption is minimal, 61.8 μW output of the fundamental was measured. Utilizing the values of the linear losses obtained from measurements, while assuming an approximate facet reflectivity of 30% and 35% transmissivity of the output objective lens, the coupling efficiency is estimated to amount to $1.8\pm0.3\%$. This low value is expected and is attributed to the thin core region used, which reduces the numerical aperture.

The SHG experiments were carried out for type-I phase matching where the input TE-polarized fundamental power couples to a TM-polarized output at the SH. The wavelength tuning curve was found by observing the SH output power, at a fixed input power, as the wavelength of the fundamental was tuned. The results are shown in Fig. 2, where a clear peak can be seen at 1600 nm indicating the location of PM conversion. In this case, the available average input power allowed 3.2 mW of the pump to be coupled into the waveguide, just inside the front facet. Modulation of the tuning curve by the Fabry–Pérot fringes of the pump is noticeable but is not pronounced due to the wide input bandwidth. The peak at which the PM takes place is shifted by 12 nm from the slab case. The shift is attributed to the influence of the two-dimensional (2D) guiding on the propagation constant of both the pump and the SH signals. This effect was confirmed through numerical simulation of the dependence of the ridge width on phase-matching wavelength. The results are illustrated in Fig. 3 where a redshift of the PM wavelength due to ridge confinement is evident.

We further investigated the control of the PM condition of the structure through temperature tuning. The wavelength tuning curve discussed above was repeated for temperatures between 15 and 40 °C. For this temperature range, the tuning slope was found to be ~0.25 nm/ °C, as illustrated by the symbols in the inset of Fig. 2. The wavelength shift is in agreement with theoretical calculations shown in the inset by the dashed line.

The spectra of both the phase-matched (SH1) and unphased-matched SH (SH2) signals, along with a typical fundamental spectrum (FN) are shown in Fig. 4. Contrary to the slab case, there was no noticeable change in the SH spectral FWHM between the phase-matched and unphase matched cases. This can be ascribed to the finite side wall roughness of the etched waveguide. Both the photolithography and plasma etching processes contribute to this roughness. In the case of slab BRW, the FWHM of the SH spectra was 0.45 nm, as predicted from the theory[6] while in the ridge case, as reported here, is 0.96 nm. From the simulations of the PM dependence on ridge width, it was established that this broadening can be caused by a variation in waveguide width of ±40 nm, as can be seen in Fig. 3. This roughness would in turn broaden the PM spectrum as well as the tuning curve. The FWHM of the tuning curve is 4.5 nm, also ap-

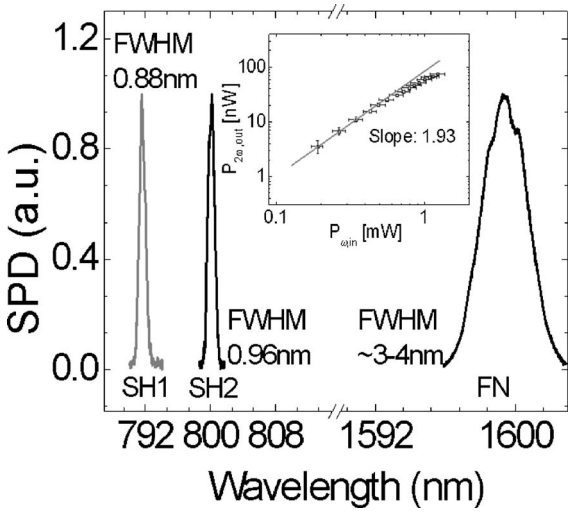

FIG. 4. Spectra of a typical input fundamental (FN), unphase-matched (SH1), and phase-matched second harmonics (SH2). The input fundamental power *vs* output second-harmonic power at the phase-matched wavelength has the expected slope of ~2 on a log-log plot (inset).

proximately twice that of the slab case. It has been previously reported that propagation losses can also contribute to this broadening.[7] However, the SH losses required to explain this FWHM need to be $>80\ \mathrm{cm}^{-1}$. This range of loss values is not conducive to this type of waveguides. It cannot be explained solely through band-tail absorption[8] for this detuning from the bandgap or through substrate leakage.[6] Further investigation through simulation of the nonlinear Schrödinger equation is required to provide a more complete picture of all the contributing effects.[9]

The second-order nonlinearity is quantified upon inspection of the SH output power versus input power. The log-log plot is shown in the inset of Fig. 4 for the PM wavelength (1600 nm). A linear fit of this curve has a slope of 1.93 confirming the quadratic dependence of the pump and SH power. The effect of the nonlinear absorption is evident by the deviation of the higher power points. Unphase-matched SH also demonstrated the quadratic dependence.

The conversion observed in this work is more efficient than the slab case as predicted. We define the conversion efficiency as $P_{\mathrm{out}}(2\omega)/P_{\mathrm{in}}(\omega)^2$, where $P_{\mathrm{out}}(2\omega)$ is the SH power just before the output facet and $P_{\mathrm{in}}(\omega)$ is the pump power just after the input facet. At low input powers for which the nonlinear absorption was minimal, the average conversion efficiency was calculated to be $8.6\pm1\%/\mathrm{W}$ compared to $0.1\%/\mathrm{W}$ for the slab. The enhancement can be attributed to the increased modal intensity provided by the 2D confinement of the ridge.

The normalized internal conversion efficiency η_0 is challenging to estimate because of the difficulty in directly measuring the SH mode loss. However, a lower bound can be estimated by assuming no loss at the SH, from Ref. 7,

$$\frac{\eta}{\eta_0} = e^{-2\alpha(\omega)L}\left\{\frac{1-e^{-[\alpha(2\omega)/2-\alpha(\omega)]L}}{[\alpha(2\omega)/2-\alpha(\omega)]L}\right\}^2. \quad (1)$$

Here, $\eta = P_{\mathrm{out}}(2\omega)/[P_{\mathrm{in}}(\omega)L]^2$ is the measured internal conversion efficiency, where the sample length L is accounted for. The parameters $\alpha(\omega)$ and $\alpha(2\omega)$ are the propagation losses of the pump and SH, respectively. For this sample, η was found to be $205\pm10\%/\mathrm{W\,cm}^2$ at 1600 nm. Assuming no loss for the SH mode and using (1), η_0 is found to be at least $600\%/\mathrm{W\,cm}^2$. This is on par or greater than numbers obtained for periodically poled lithium niobate (PPLN).[7,10] The actual value of η_0 is expected to be much larger because the SH loss can be significant given the proximity of the PM wavelength to the bandgap of the materials. Also, 100% collection efficiency of the output objective is assumed in these calculations.

Despite being the initial experimental demonstration, this value is within an order of magnitude of other reported values in AlGaAs waveguides such as birefringent phase matching,[11] modal phase matching,[1] and quasi-phase matching.[3] This demonstrates the efficiency of the internal conversion process through utilizing the nonlinear coefficient of AlGaAs which is higher than popular nonlinear crystals such as PPLN. Values of bulk external conversion, defined as as the ratio of the fundamental power before the input objective and SH power after the output objective, are limited significantly by several factors. Firstly, the low coupling efficiency greatly reduces the useable fundamental power. Secondly, the etch process can be optimized to reduce the scattering losses. Lastly, the interaction length can also be maximized through reducing walk off between the interacting waves. It has been shown that the group-velocity mismatch can be tuned by appropriate structure design.[6]

In conclusion, we report the observation of efficient phase matching using monolithic AlGaAs based ridge Bragg-reflection waveguides. The PM wavelength was at 1600 nm with a FWHM of 4.5 nm. The PM position was tuned by 10 nm over a temperature range of 20–60 °C resulting in a tuning slope of 0.25 nm/°C. The conversion efficiency is found to be $8.6\%/\mathrm{W}$ and internal conversion efficiency is $205\%/\mathrm{W\,cm}^2$. The flexibility and promise of this technique provide ample room for improvement through optimized sample design and improved fabrication process.

[1] K. Moutzouris, S. Venugopal Rao, M. Ebrahimzadeh, A. De Rossi, M. Calligaro, V. Ortiz, and V. Berger, Appl. Phys. Lett. **83**, 620 (2003).
[2] A. Fiore, S. Janz, L. Delobel, P. van der Meer, P. Bravetti, V. Berger, E. Rosencher, and J. Nagle, Appl. Phys. Lett. **72**, 2942 (1998).
[3] K. Zeaiter, D. C. Hutchings, R. M. Gwilliam, K. Moutzouris, S. V. Rao, and M. Ebrahimzadeh, Opt. Lett. **28**, 911 (2003).
[4] A. S. Helmy, Opt. Express **14**, 1243 (2006).
[5] A. S. Helmy, B. Bijlani, and P. Abolghasem, Opt. Lett. **32**, 2399 (2007).
[6] B. R. West and A. S. Helmy, IEEE J. Sel. Top. Quantum Electron. **12**, 431 (2006).
[7] M. L. Bortz, S. J. Field, M. M. Fejer, D. W. Nam, R. G. Waarts, and D. F. Welch, IEEE J. Quantum Electron. **30**, 2953 (1994).
[8] B. Monemar, K. K. Shih, and G. D. Pettit, J. Appl. Phys. **47**, 2604 (1976).
[9] S. J. Wagner, A. A. Muhairi, J. S. Aitchison, and A. S. Helmy, IEEE J. Sel. Top. Quantum Electron. **44**, 424 (2008).
[10] K. R. Parameswaran, R. K. Route, J. R. Kurz, R. V. Roussev, M. M. Fejer, and M. Fujimura, Opt. Lett. **27**, 179 (2002).
[11] K. Moutzouris, S. Venugopal Rao, M. Ebrahimzadeh, A. De Rossi, V. Berger, M. Calligaro, and V. Ortiz, Opt. Lett. **26**, 1785 (2001).